Dynamic-Phasor-Based Nonlinear Modelling of AC Islanded Microgrids Under Droop Control

Mariani, Valerio; Vasca, Francesco; Guerrero, Josep M.

Published in:
Proceedings of the 11th International Multi-Conference on Systems, Signals & Devices, SSD 2014

DOI (link to publication from Publisher):
10.1109/SSD.2014.6808872

Publication date:
2014

Document Version
Early version, also known as pre-print

Dynamic-Phasor-Based Nonlinear Modelling of AC Islanded Microgrids Under Droop Control

V. Mariani and F. Vasca
Department of Engineering
University of Sannio
Piazza Roma 21, 82100 Benevento, Italy
Email: {vmariani,vasca}@unisannio.it

J. M. Guerrero
Department of Energy Technology
Aalborg University
Pontoppindastraede 101, 9100 Aalborg, Denmark
Email: joz@et.aau.dk

***Abstract*—Droop controlled inverters are widely used in islanded microgrids to interface distributed energy resources and to provide for the loads active and reactive powers demand. In this scenario, an important issue is to assess the stability of the microgrids taking into account the network and currents dynamics that are also affected by the control parameters. This paper shows how a dynamic phasor approach can be used to derive a closed loop model of the microgrid and then to perform an eigenvalues analysis that highlights how instabilities arise for suitable values of the frequency droop control parameter. Further, it is shown that the full order system is well approximated by a reduced order system which captures the inverters phase and line currents dynamics.**

I. INTRODUCTION

Modern power microgrids consist of a continuously increasing number and variety of different and distributed power sources and loads connected via various topologies. The droop technique is widely used to control microgrid inverters to properly interface the distributed power resources to the electrical network and to support for the active and reactive power loads demand [1], [2], [3]. Because of the nonlinearity of the control technique, even in presence of small microgrids with few inverters, the closed loop model of such systems may become very complex. Neverthless, a precise assessment of the stability of the microgrids is very important. In the past this was usually tackled via a small-signal analysis performed by neglecting the dynamics of the line and loads and/or of the currents [4], [5], [6], [7], [8]. This approach is usually justified by a-priori because of the low-pass characteristic of the power measurement block and because of the choice of a suitabily small frequency droop parameter. Then, the resulting approximated system is validated by experimental simulations. Recently, many papers have proposed a dynamic phasors approach to take into account for the network and for the currents dynamics, see among the others [9]. Further, some efforts have been also put for a more theoretically rigorous analysis of the interesting issues related to the control and stability of distributed generation systems with droop controlled inverters [10] also with a large signals perspective [11], [12]. In this paper, a model of an AC microgrid consisting of two inverters connected via a resistive-inductive line and of two local resistive-inductive loads is drawn by using a dynamic phasor representation of the Kirchhoff voltage and current laws governing the system. Also, a singular perturbation approach is used in order to draw a reduced order system where the loads dynamics are assumed to be at steady-state. Then, the closed loop equations of the full order model are used to compute the equilibrium point of the system and then to assess its local stability. An eigenlocus analysis that highlights the impact of the control parameters on the small-signal stability of the AC microgrid under investigation is also performed. Simulations showing that the reduced order system well approximates the full order system are reported. The rest of the paper is organized as follows. In Sec. II an open-loop model of the microgrid under investigation is derived in the domain of dynamic phasors by assuming local angle reference frames. Then, in Sec. III the closed-loop full order and reduced order models of the system are drawn. A numerical analysis of the full order model showing the time evolutions of the currents, the powers, the angle delay between the two inverters, the inverter frequencies, the eigenlocus plotted for increasing frequency control parameter is presented in Sec. IV. Further, in Sec. IV, the full order model and the reduced order model are compared and numerical simulation results shows that the time domain evolution of the full order model's line current is well approximated by that of the reduced order model as well as the time domain evolution of the full order model's angle and the time domain evolution of the reduced order model's angle. Sec. V concludes the paper.

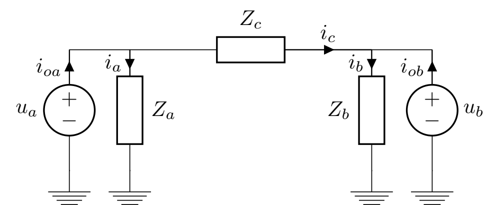

Fig. 1. AC microgrid in islanded-mode with two inverters and two local loads.

II. AC MICROGRID MODEL

The AC microgrid under investigation is depicted in Fig. 1. Two inverters are connected by means of a resistive-inductive line $Z_c = R_c + \jmath\omega L_c$ and to the corresponding resistive-inductive local loads $Z_a = R_a + \jmath\omega L_a$ and $Z_b = R_b + \jmath\omega L_b$. We assume that the voltage u_k provided by the k-th inverter, the corresponding k-th output current i_{ok} and the corresponding k-th local load current i_k are

$$u_k = \sqrt{2}\, U_k \cos\theta_k, \tag{1a}$$
$$i_{ok} = \sqrt{2}\, I_{ok} \cos(\theta_k + \varphi_k), \tag{1b}$$
$$i_k = \sqrt{2}\, I_k \cos(\theta_k + \phi_k), \tag{1c}$$

with $k = a, b$ and where U_k, θ_k, I_{ok} and I_k are the time-varying voltage amplitude, the time-varying angle, the time-varying output and load currents amplitude of the k-th inverter determined with respect the k-th local reference frame. Further, φ_k and ϕ_k are the time-varying angle delays of the k-th output inverter current and load current with respect to the corresponding voltages instantaneous phases θ_k. Both U_k and θ_k are determined by the frequency and amplitude droop laws. Assume, then, that the line current i_c is given by

$$i_c = \sqrt{2}\, I_c \cos\theta_c = \sqrt{2}\, I_c \cos(\theta_a + x_a), \tag{2}$$

where θ_c is the time-varying angle determined with respect to the local line reference frame and $x_a = \theta_c - \theta_a$ is the angle delay between the angle of u_a and the angle of the line current i_c. The Kirchhoff voltage laws of the circuit depicted in Fig. 1 allow to write the following equations

$$L_k \frac{d}{dt} i_k = - R_k i_k + u_k, \tag{3a}$$
$$L_c \frac{d}{dt} i_c = - R_c i_c + u_a - u_b, \tag{3b}$$

where $k = a, b$, and the Kirchhoff current laws determine

$$i_{oa} = i_a + i_c, \tag{4a}$$
$$i_{ob} = i_b - i_c. \tag{4b}$$

A dynamic phasor representations of (3) and (4) is obtained by chosing θ_k as reference time-varying angle for each k-th inverter, with $k = a, b$, and by chosing θ_a as the reference time-varying angle for the line current i_c. Each u_k, i_{ok}, i_k and i_c is expressed in terms of its own corresponding dynamic phasor as

$$u_k = \sqrt{2}\, \mathfrak{Re}\{U_k e^{\jmath\theta_k}\}, \tag{5a}$$
$$i_{ok} = \sqrt{2}\, \mathfrak{Re}\{(i_{ok}^d + \jmath i_{ok}^q) e^{\jmath\theta_k}\}, \tag{5b}$$
$$i_k = \sqrt{2}\, \mathfrak{Re}\{(i_k^d + \jmath i_k^q) e^{\jmath\theta_k}\}, \tag{5c}$$
$$i_c = \sqrt{2}\, \mathfrak{Re}\{(i_c^d + \jmath i_c^q) e^{\jmath\theta_a}\}, \tag{5d}$$

where $k = a, b$. Notice that the direct i_c^d and quadrature i_c^q component of the line current are defined with respect a rotating reference frame given by the angle θ_a of the voltage u_a. Define $\delta = \theta_a - \theta_b$ as the angle delay existing between the voltage u_a and the voltage u_b. Then, by using (5) in (3) and by solving for any $\theta_k \in [0, 2\pi)$ [11] we get

$$L_k \frac{d}{dt} i_k^d = - R_k i_k^d + \frac{d}{dt}\theta_k\, L_k i_k^q + U_k, \tag{6a}$$
$$L_k \frac{d}{dt} i_k^q = - \frac{d}{dt}\theta_k\, L_k i_k^d - R_k i_k^q, \tag{6b}$$
$$L_c \frac{d}{dt} i_c^d = - R_c i_c^d + \frac{d}{dt}\theta_a\, L_c i_c^q + U_a - U_b \cos\delta, \tag{6c}$$
$$L_c \frac{d}{dt} i_c^q = - \frac{d}{dt}\theta_a\, L_c i_c^d - R_c i_c^q + U_b \sin\delta, \tag{6d}$$

where $k = a, b$, and by using (5) in (4) and by solving for any $\theta_k \in [0, 2\pi)$ we get

$$i_{oa}^d = i_a^d + i_c^d, \tag{7a}$$
$$i_{oa}^q = i_a^q + i_c^q, \tag{7b}$$
$$i_{ob}^d = i_b^d - i_c^d \cos\delta + i_c^q \sin\delta, \tag{7c}$$
$$i_{ob}^q = i_b^q - i_c^q \cos\delta - i_c^d \sin\delta. \tag{7d}$$

Eq. (6) show that the currents dynamics are affected by those of θ_k. Particularly, since each $(d/dt)\theta_k$, with $k = a, b$, is determined with the standard frequency droop law, the contribution of the inductance L_j, with $j = k, c$, to each corresponding current dynamic depends on a fixed frequency term ωL_j, where ω is the frequency reference for both frequency droop laws, and on a time-varying term. In turn, this last depends on the frequency control parameter m_k and on the measured active power P_k. Notice that ωL_j corresponds to the j-th inductive reactance if the microgrid in Fig. 1 admits a steady-state regime. Thus, in order to neglect the network dynamics one has to ensure that the j-th nominal reactance ωL_j is much greater than the product $m_k P_k L_j$, with $k = a, b$, $j = k, c$, and where P_k is time-dependent.

III. Closed Loop Model

The closed loop model of (6) is obtained by determining the amplitude U_k and the frequency $(d/dt)\theta_k$ of each k-th voltage, with $k = a, b$, according to the frequency and voltage droop laws

$$\frac{d}{dt}\theta_k = \omega + m_k(\bar{P}_k - P_k), \tag{8a}$$
$$U_k = \bar{U}_k + n_k(\bar{Q}_k - Q_k), \tag{8b}$$

where ω is the reference frequency for both inverters, $\bar{U}_k$ is the k-th voltage reference, m_k and n_k is the k-th frequency and voltage droop coefficients, $\bar{P}_k$ and $\bar{Q}_k$ is the k-th active and reactive power references, P_k and Q_k are the k-th "instantaneous" active and reactive powers provided by the k-th inverter, with $k = a, b$. Each k-th P_k and Q_k is given by

$$P_k = \mathfrak{Re}\{U_k (i_{ok}^d + \jmath i_{ok}^q)^*\} = U_k i_{ok}^d, \tag{9a}$$
$$Q_k = \mathfrak{Im}\{U_k (i_{ok}^d + \jmath i_{ok}^q)^*\} = -U_k i_{ok}^q, \tag{9b}$$

where the superscript '$*$' indicates the complex conjugate and $k = a, b$. If the circuit in Fig. 1 with the inverter subject to droop control admits a sinusoidal regime, (9) correspond to the classical definitions of active and reactive powers. By using (9b) in (8b) we obtain

$$U_k = \frac{\bar{U}_k + n_k \bar{Q}_k}{1 - n_k\, i_{ok}^q} \tag{10}$$

where i_{ok}^q is given by (7) and $k = a, b$. In turn, the corresponding frequency $(d/dt)\theta_k$ of the k-th inverter is obtained by substituting (10) with (9a) in (8a):

$$\frac{d}{dt}\theta_k = \omega + m_k \left(\bar{P}_k - U_k\, i_{ok}^d\right), \tag{11}$$

being i_{ok}^d and i_{ok}^q defined in (7), U_k given by (10) and $k = a, b$. Then, by substituting (11) and (10) in (6) and since $(d/dt)\delta = (d/dt)(\theta_a - \theta_b)$, the closed loop model of the microgrid represented in Fig. 1 is

$$\begin{aligned}
\frac{L_a}{R_a}\frac{d}{dt} i_a^d =& - i_a^d + \frac{1}{R_a} U_a + m_a \left(\bar{P}_a - U_a\, i_{oa}^d\right) \frac{L_a}{R_a} i_a^q \\
&+ \frac{\omega L_a}{R_a} i_a^q, && (12a)\\
\frac{L_a}{R_a}\frac{d}{dt} i_a^q =& - \frac{\omega L_a}{R_a} i_a^d - i_a^q - m_a \left(\bar{P}_a - U_a\, i_{oa}^d\right) \frac{L_a}{R_a} i_a^d, && (12b)\\
\frac{L_b}{R_b}\frac{d}{dt} i_b^d =& - i_b^d + \frac{1}{R_b} U_b + m_b \left(\bar{P}_b - U_b\, i_{ob}^d\right) \frac{L_b}{R_b} i_b^q \\
&+ \frac{\omega L_b}{R_b} i_b^q, && (12c)\\
\frac{L_b}{R_b}\frac{d}{dt} i_b^q =& - \frac{\omega L_b}{R_b} i_b^d - i_b^q - m_b \left(\bar{P}_b - U_b\, i_{ob}^d\right) \frac{L_b}{R_b} i_b^d, && (12d)\\
\frac{L_c}{R_c}\frac{d}{dt} i_c^d =& - i_c^d + \frac{\omega L_c}{R_c} i_c^q + m_a \left(\bar{P}_a - U_a\, i_{oa}^d\right) \frac{L_c}{R_c} i_c^q \\
&+ \frac{1}{R_c} U_a - \frac{1}{R_c} U_b \cos\delta, && (12e)\\
\frac{L_c}{R_c}\frac{d}{dt} i_c^q =& - \frac{\omega L_c}{R_c} i_c^d - i_c^q - m_a \left(\bar{P}_a - U_a\, i_{oa}^d\right) \frac{L_c}{R_c} i_c^d \\
&+ \frac{1}{R_c} U_b \sin\delta, && (12f)\\
\frac{d}{dt}\delta =& m_a \left(\bar{P}_a - U_a\, i_{oa}^d\right) - m_b \left(\bar{P}_b - U_b\, i_{ob}^d\right), && (12g)
\end{aligned}$$

where i_{ok}^d, i_{ok}^q and U_k with $k = a, b$ are given by (7) and (10) respectively. Typical values of the loads inductances L_k and resistances R_k, where $k = a, b$, allow to assume

$$\frac{L_a}{R_a}, \frac{L_b}{R_b} \ll \frac{L_c}{R_c}. \tag{13}$$

Therefore, by applying a singular perturbation approach [13] to (12) with (7) and (10) one obtains

$$\begin{aligned}
0 &= -z_a^d + \frac{\omega L_a}{R_a}\, z_a^q + \frac{1}{R_a}\frac{\bar{U}_a + n_a \bar{Q}_a}{1 - n_a (z_a^q + z_c^q)}, && (14a)\\
0 &= -\frac{\omega L_a}{R_a}\, z_a^d - z_a^q, && (14b)\\
0 &= -z_b^d + \frac{\omega L_b}{R_b}\, z_b^q + \frac{1}{R_b}\frac{\bar{U}_b + n_b \bar{Q}_b}{1 - n_b (z_b^q - z_c^q \cos\delta_z - z_c^d \sin\delta_z)}, && (14c)\\
0 &= -\frac{\omega L_b}{R_b}\, z_b^d - z_b^q, && (14d)
\end{aligned}$$

where we have used z and δ_z to indicate the currents and the angle of the reduced order model respectively, we have used singularly perturbed variables in (7) and where the assumption of small ratios L_k/R_k does not imply small $\omega L_k/R_k$. Since the voltages amplitudes U_a and U_b are positive, from (10) and by solving (14b), (14d) for z_a^d and z_b^d respectively and then substituting in (14a) and (14c) one obtains

$$\begin{aligned}
0 =& (z_a^q)^2 - \frac{1}{n_a}(1 - n_a z_c^q) z_a^q - \frac{\omega L_a}{n_a Z_a^2}(\bar{U}_a + n_a \bar{Q}_a), && (15a)\\
z_a^d =& -\frac{R_a}{\omega L_a} z_a^q, && (15b)\\
0 =& (z_b^q)^2 - \frac{1}{n_b}[1 + n_b (z_c^q \cos\delta_z + z_c^d \sin\delta_z)] z_b^q \\
&- \frac{\omega L_b}{n_b Z_b^2}(\bar{U}_b + n_b \bar{Q}_b), && (15c)\\
z_b^d =& -\frac{R_b}{\omega L_b} z_b^q, && (15d)
\end{aligned}$$

where $Z_a^2 = R_a^2 + (\omega L_a)^2$ and $Z_b^2 = R_b^2 + (\omega L_b)^2$ are the squared modulus of the complex load impedances Z_a and Z_b respectively. From (15), for sufficiently small n_a and n_b, one obtains the expected approximations

$$\begin{aligned}
z_a^d \approx& \frac{R_a}{Z_a^2}(\bar{U}_a + n_a \bar{Q}_a), && (16a)\\
z_a^q \approx& -\frac{\omega L_a}{Z_a^2}(\bar{U}_a + n_a \bar{Q}_a), && (16b)\\
z_b^d \approx& \frac{R_b}{Z_b^2}(\bar{U}_b + n_b \bar{Q}_b), && (16c)\\
z_b^q \approx& -\frac{\omega L_b}{Z_b^2}(\bar{U}_b + n_b \bar{Q}_b). && (16d)
\end{aligned}$$

The reduced order model of (12) is obtained by substituting the solutions of (15) into (7), in

$$U_{k,z} = \frac{\bar{U}_k + n_k \bar{Q}_k}{1 - n_k\, z_{ok}^q}, \tag{17}$$

for $k = a, b$ and then in (12e)-(12g):

$$\begin{aligned}
\frac{L_c}{R_c}\frac{d}{dt}\, z_c^d =& - z_c^d + \frac{\omega L_c}{R_c} z_c^q + m_a \left(\bar{P}_a - U_{a,z}\, z_{oa}^d\right) \frac{L_c}{R_c} z_c^q \\
&+ \frac{1}{R_c} U_{a,z} - \frac{1}{R_c} U_{b,z} \cos\delta_z, && (18a)\\
\frac{L_c}{R_c}\frac{d}{dt}\, z_c^q =& - \frac{\omega L_c}{R_c} z_c^d - z_c^q - m_a \left(\bar{P}_a - U_{a,z}\, z_{oa}^d\right) \frac{L_c}{R_c} z_c^d \\
&+ \frac{1}{R_c} U_{b,z} \sin\delta_z, && (18b)\\
\frac{d}{dt}\delta_z =& m_a \left(\bar{P}_a - U_{a,z}\, z_{oa}^d\right) - m_b \left(\bar{P}_b - U_{b,z}\, z_{ob}^d\right). && (18c)
\end{aligned}$$

The numerical results in next Section will show scenarios for which the reduced order model (18) can be useful for the analysis of islanded microgrids under droop control.

IV. Simulation Results

The simulations have been carried out by considering the following realistic values of the controls, loads and line parameters [5] for the microgrid depicted in Fig. 1: $m_a = 5 \cdot 10^{-4}$ rad/sW, $n_a = 5 \cdot 10^{-4}$ V/VAr, $\bar{P}_a = 806$ W, $\bar{Q}_a = 384$ VAr, $\bar{U}_a = 127$ V, $R_a = 13\ \Omega$, $L_a = 16$ mH, $m_b = 5 \cdot 10^{-4}$ rad/sW, $n_b = 5 \cdot 10^{-4}$ V/VAr, $\bar{P}_b = 750$ W, $\bar{Q}_b = 375$ VAr, $\bar{U}_b = 130$ V, $R_b = 25\ \Omega$, $L_b = 35$ mH, $R_c = 0.5\ \Omega$, $L_c = 8$ mH, $\omega = 2\pi\, 60$ rad/s. The equilibrium point of the closed loop system is $i_a^{d,\text{eq}} = 8.1$ A, $i_b^{d,\text{eq}} = 4.1$ A, $i_a^{q,\text{eq}} = -3.7$ A, $i_b^{q,\text{eq}} = -2.1$ A, $i_c^{d,\text{eq}} = -1.7$ A, $i_c^{q,\text{eq}} = 0.7$ A, $\delta^{\text{eq}} = -0.0368$ rad and the eigenvalues of the system's Jacobian computed around such an equilibrium point are

$$\lambda_{1,2} = -\,816.69 \pm \jmath 375.1, \tag{19a}$$

$$\lambda_3 = -\,5.39, \tag{19b}$$

$$\lambda_{4,5} = -\,60.15 \pm \jmath 368.59, \tag{19c}$$

$$\lambda_{6,7} = -\,724.91 \pm \jmath 375.91, \tag{19d}$$

which show that the system is locally stable for the particular choice of the line, control and load parameteres above mentioned. Fig. 2 and Fig. 3 show the time domain evolution of the local loads direct and quadrature currents and the time domain evolution of the inverters and line direct and quadrature currents respectively. Fig. 3 particularly shows the presence of fast and slow modes in the inverters and line currents dynamics. Comparing Fig. 2 and Fig. 3 one can notice how the loads currents evolve on the same small temporal scale of the fast modes which affect the inverters and line currents. In Fig. 4 are reported the time evolutions of the active P_a, P_b, and reactive powers Q_a, Q_b, of each inverter. Fig. 5 shows the time domain evolution of the difference $\delta = \theta_a - \theta_b$ between the angle θ_a and the angle θ_b. The inverters start with the same angle, that is $\delta(0) = 0$, and in order to provide for the required active and reactive powers according to the corresponding reference values, at steady-state a non-zero angle difference is needed. Clearly, this depends also by the local loads. In Fig. 6 it is shown the time evolution of the instantaneous frequencies $(d/dt)\theta_a$ (solid line) and $(d/dt)\theta_b$ (dashed line) determined by the frequency droop laws. Each $(d/dt)\theta_k$ starts from the corresponding initial value given by $\omega + m_k \bar{P}_k$, where $k = a, b$. Then, both $(d/dt)\theta_a$ and $(d/dt)\theta_b$ converge to the same steady-state value given by the frequency reference $\omega = 2\pi\, 60$ rad/s since also P_a and P_b converge to $\bar{P}_a$ and $\bar{P}_b$ respectively. Fig. 7 shows the eigenlocus for $m_a \in [5 \cdot 10^{-4}, 5 \cdot 10^{-2}]$. For each $m_a \in [5 \cdot 10^{-4}, 5 \cdot 10^{-2}]$ the new equilibrium point, given by the solution of (12) obtained setting all the derivative terms to zero, has been computed and then used to determine the eigenvalues of the system's Jacobian. As it is shown, by increasing the frequency control parameter m_a some of the eigenvalues become positive real, and for $m_a \geq 2.4 \cdot 10^{-2}$ the system is unstable. Fig. 7 and (19) show that, for $m_a = 5 \cdot 10^{-4}$, the linearized dynamic is approximately given by a third order system obtained by neglecting the fast eigenvalues $\lambda_{1,2}$ and $\lambda_{6,7}$. The simulations

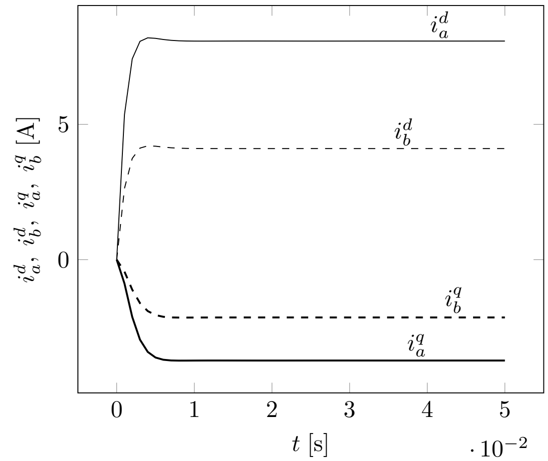

Fig. 2. Time domain evolution of the direct components i_a^d (solid line) and i_b^d (dashed line) of the load a and b currents and quadrature components i_a^q (solid thick line) and i_b^q (dashed thick line) of the load a and b currents for zero initial conditions, for $m_a = 5 \cdot 10^{-4}$.

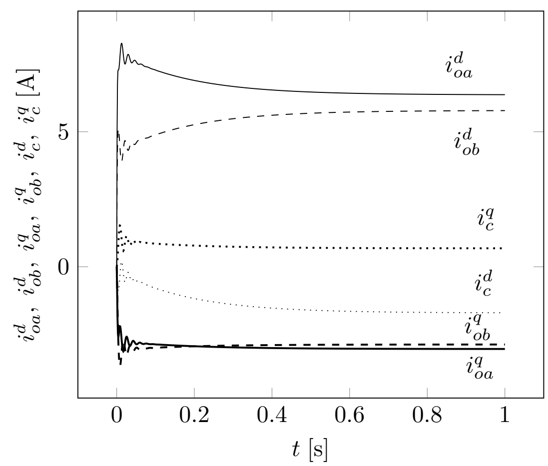

Fig. 3. Time domain evolution of the direct components i_{oa}^d (solid line), i_{ob}^d (dashed line), i_c^d (dotted line) and quadrature component i_{oa}^q (solid thick line), i_{ob}^q (dashed thick line), i_c^q (dotted thick line) of the inverters' and line direct and quadrature currents for zero initial conditions, for $m_a = 5 \cdot 10^{-4}$.

in Fig. 8 allow to verify that such an approximation is valid also for large signals for $m_a = 5 \cdot 10^{-4}$. On the contrary, Fig. 9 and Fig. 10 show that for $m_a = 2.3 \cdot 10^{-2}$ the error between the reduced order model (18) and the full order model (12) increases. On the other hand, as the eigenlocus of the reduced order system depicted in Fig. 11 shows, the reduced model predicts the instability occurring for the same value of the frequency control parameter $m_a = 2.4 \cdot 10^{-2}$ of the first inverter for which the full order model is unstable. Finally, in Fig. 12 it is reported the eigenlocus of the reduce order system for increasing ratios L_c/R_c and for $m_a = 2.4 \cdot 10^{-2}$. As the ratio L_c/R_c increases, the real part of the complex conjugate eigenvalues become positive and the reduced order system is unstable.

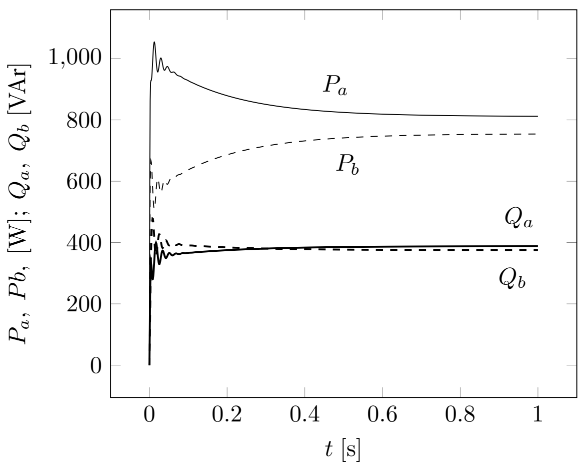

Fig. 4. Time domain evolution of the active powers P_a (solid line), P_b (dashed line) and reactive powers Q_a (solid thick line), Q_b (dashed thick line) provided by the inverters, for $m_a = 5 \cdot 10^{-4}$.

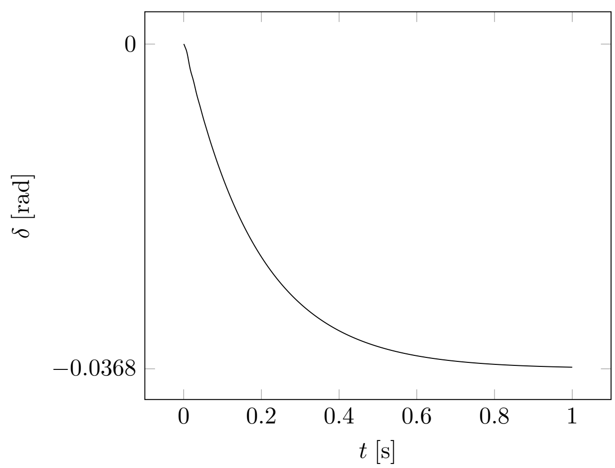

Fig. 5. Time domain evolution of the angle delay δ existing between the voltage u_a and the voltage u_b for zero initial conditions, for $m_a = 5 \cdot 10^{-4}$.

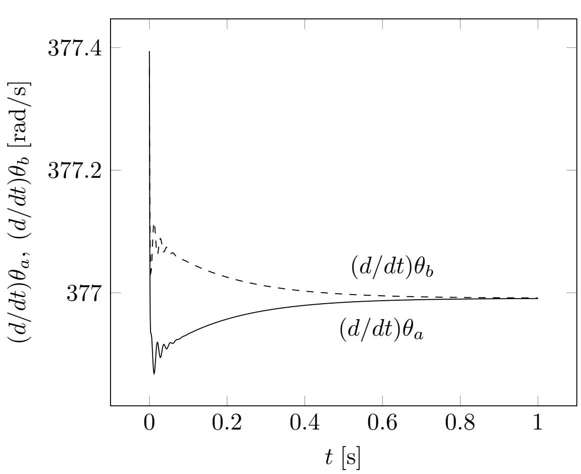

Fig. 6. Time domain evolution of the frequency $(d/dt)\theta_a$ (solid line) and $(d/dt)\theta_b$ (dashed line) of the voltage u_a and the voltage u_b provided by the microgrid inverters, for $m_a = 5 \cdot 10^{-4}$.

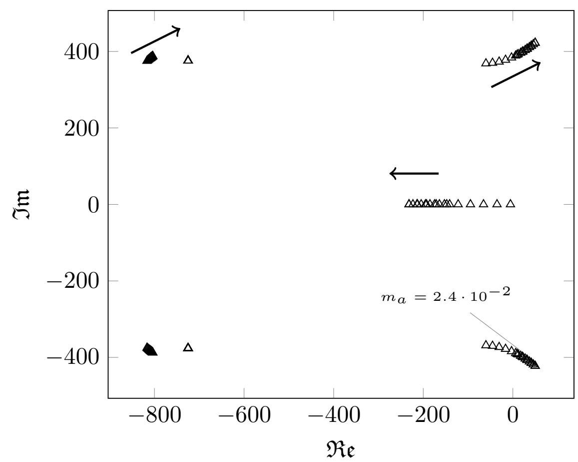

Fig. 7. Eigenlocus of the linearized system around the equilibrium point for $m_a \in [5 \cdot 10^{-4}, 5 \cdot 10^{-2}]$.

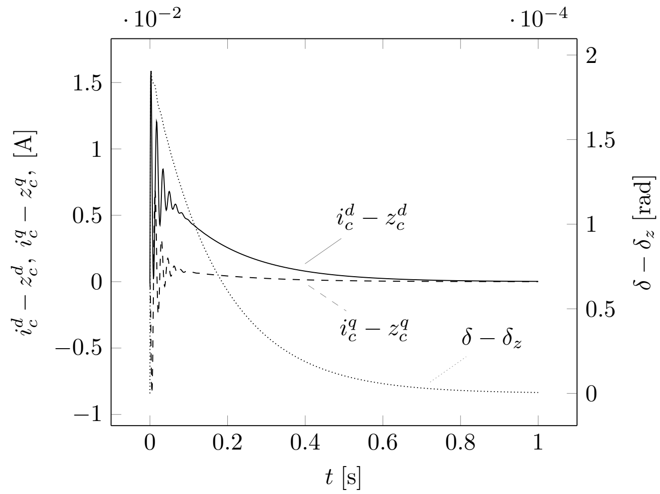

Fig. 8. Time evolutions of the difference $i_c^d - z_c^d$ (solid line) between the full order model direct line current i_c^d and the reduced order model direct line current z_c^d, of the difference $i_c^q - z_c^q$ (dashed line) between the full order model quadrature line current i_c^q and the reduced order model quadrature line current z_c^q and of the difference $\delta - \delta_z$ (dotted line) between the full order model angle delay δ and the reduced order model angle delay δ_z, for $m_a = 5 \cdot 10^{-4}$.

V. Conclusions

The dynamic phasors approach to model two droop controlled inverters forming a microgrid allows to compute the equilibrium points of the closed loop system and to carry out an eigenvalue analysis showing that for some values of the frequency droop control parameter m_a the system becomes unstable. The proposed technique allows also to assess that for sufficiently small values of m_a the large signals dynamics are well approximated by those of a reduced order model derived by neglecting the loads dynamics, that is by applying a singular perturbation approach to the original dynamic phasor model. The approximation becomes worse as m_a increases but the reduced order model is still able to predict the instability. The same technique and similar considerations can be operated

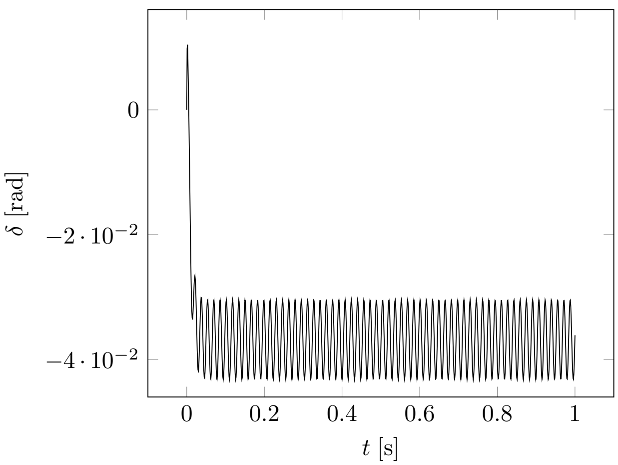

Fig. 9. Time domain evolution of the full order model angle delay δ, for $m_a = 2.3 \cdot 10^{-2}$.

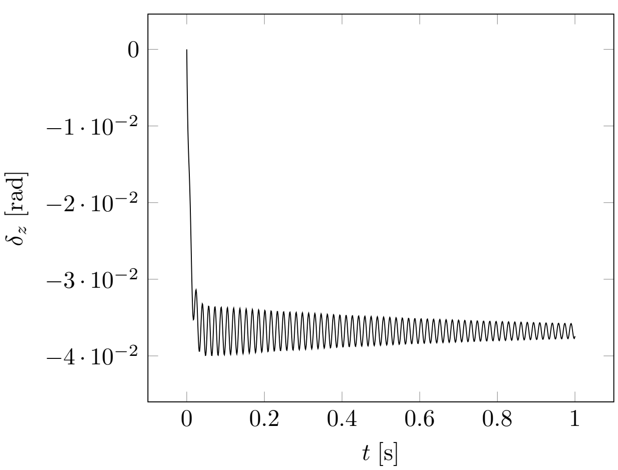

Fig. 10. Time domain evolution of the reduced order model angle delay δ_z, for $m_a = 2.3 \cdot 10^{-2}$.

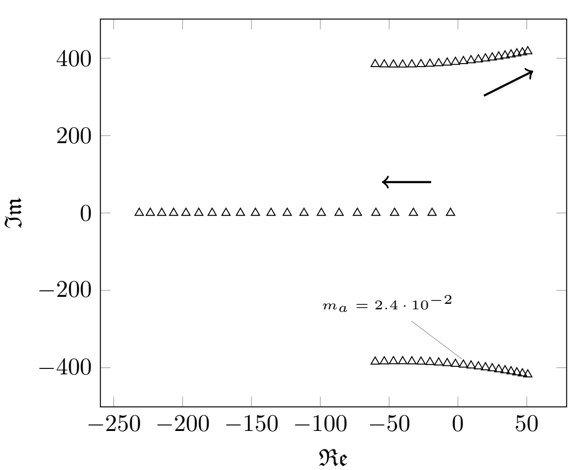

Fig. 11. Eigenlocus of the reduced order model linearized around the equilibrium point for $m_a \in [5 \cdot 10^{-4}, 5 \cdot 10^{-2}]$.

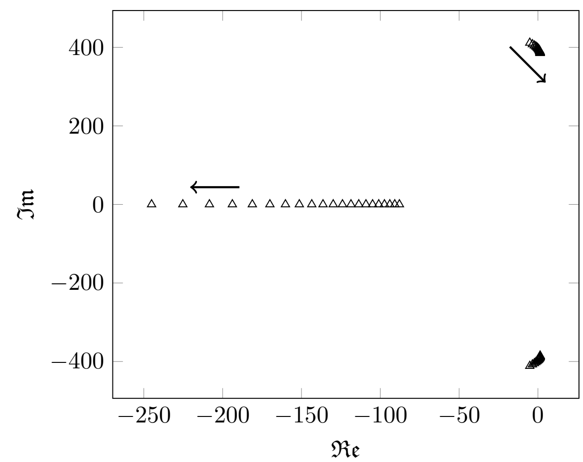

Fig. 12. Eigenlocus of the linearized reduced order system around the equilibrium point for $L_c/R_c \in [0.5, 1.5] \cdot (L_c/R_c)_{\text{nom}}$ s and $m_a = 2.4 \cdot 10^{-2}$.

with different values of the remaining parameters.

References

[1] J. M. Guerrero, M. Chandorkar, T.-L. Lee, and P. C. Loh, "Advanced Control Architectures for Intelligent Microgrids-Part I: Decentralized and Hierarchical Control," *IEEE Trans. on Industrial Electronics*, vol. 60, no. 4, pp. 1254–1262, 2013.

[2] Q.-C. Zhong, "Robust Droop Controller for Accurate Proportional Load Sharing Among Inverters Operated in Parallel," *IEEE Trans. on Industrial Electronics*, vol. 60, no. 4, pp. 1281–1290, 2013.

[3] Y. Mohamed and E. El-Saadany, "Adaptive Decentralized Droop Controller to Preserve Power Sharing Stability of Paralleled Inverters in Distributed Generation Microgrids," *IEEE Trans. on Power Electronics*, vol. 23, no. 6, pp. 2806–2816, 2008.

[4] E. A. A. Coelho, P. C. Cortizo, and P. F. D. Garcia, "Small Signal Stability for Single Phase Inverter Connected to Stiff AC System," in *Proc. of the 34th Industry Applications Conference*, vol. 4, Phoenix, Arizona, USA, October 1999, pp. 2180–2187.

[5] ——, "Small-signal stability for parallel-connected inverters in stand-alone ac supply systems," *IEEE Trans. on Industry Applications*, vol. 38, no. 2, pp. 533–542, March/April 2002.

[6] J. M. Guerrero, L. G. de Vicuña, J. Matas, M. Castilla, and J. Miret, "A Wireless Controller to Enhance Dynamic Performance of Parallel Inverters in Distibuted Generation Systems," *IEEE Trans. on Power Electronics*, vol. 19, no. 5, pp. 1205–1213, 2004.

[7] N. Pogaku, M. Prodanovic, and T. C. Green, "Modeling, analysis and testing of autonomous operation of an inverter-based microgrid," *IEEE Trans. on Power Electronics*, vol. 22, no. 2, pp. 613–625, March 2007.

[8] W. Yao, M. Chen, J. Matas, J. M. Guerrero, and Z. M. Qian, "Design and Analysis of the Droop Control Method for Parallel Inverters Considering the Impact of the Complex Impedance on the Power Sharing," *IEEE Trans. on Industrial Electronics*, vol. 58, no. 2, pp. 576–588, 2011.

[9] L. Wang, X. Q. Guo, H. R. Gu, W. Y. Wu, and J. M. Guerrero, "Precise Modeling Based on Dynamic Phasors for Droop-Controlled Parallel-Connected Inverters," in *IEEE International Symposium on Industrial Electronics*, 2012, pp. 475–480.

[10] J. W. S.-Porco, F. Dorfler, and F. Bullo, "Synchronization and Power Sharing for Droop-Controlled Inverters in Islanded Microgrids," *Automatica*, vol. 49, no. 9, pp. 2603–2611, 2013.

[11] V. Mariani and F. Vasca, "Stability Analysis of Droop Controlled Inverters via Dynamic Phasors and Contraction Theory," in *Proc. of the 12th European Control Conference*, Zurich, Switzerland, July 2013.

[12] ——, "Partial Contraction Analysis for Droop Controlled Inverters," in *Proc. of the 3rd International Conference on Systems and Control*, Algiers, Algeria, October 2013.

[13] H. K. Khalil, *Nonlinear Systems*, 3rd ed. New Jersey: Prentice Hall, 2002.